Theoretical and Experimental Investigation of Finline Discontinuities

MARYLINE HELARD, JACQUES CITERNE, ODILE PICON, AND VICTOR FOUAD HANNA

Abstract—**The dominant and the first-five higher order modes in a unilateral finline are precisely described from a thorough spectral-domain approach. Then, using the modal analysis, coupling coefficients between eigenmodes at a discontinuity that have to be introduced into the scattering matrix formulation are directly computed in the spectral-domain, and, consequently, the equivalent circuit parameters of the discontinuity are determined. Finally, finline discontinuities often used for impedance transformation are investigated and a good agreement between theoretical and experimental results is reported.**

I. Introduction

THE FIELD THEORETICAL solution of finline discontinuities presents a complex problem. This explains the small number of concise and rigorous attempts of analyses reported in the recent literature [1].

In fact, the major complexity for efficient and accurate analysis of single or complex discontinuities in finline structures lies in the necessary treatment of hybrid eigenmodes to which there is no closed-form solution.

Firstly, the modal analysis [2] has been applied [3] to single and double steps in the finline slot width, while the characterization of uniform finline structures was obtained by the moment mode-matching technique [4].

This pioneering work provided an insight into CAD potentialities of integrated millimeter-wave finline circuits [5] that such a field theoretical solution could provide. However, a hasty model in terms of equivalent circuits prevents an unbiased evaluation of computed intermediate field parameters.

A. Beyer and I. Wolff [6] used a nearly similar approach of the finline treatment and solved the discontinuity problem by a flexible and elegant combination of the moment mode-matching technique and the modal analysis.

In solving the problem of the rectangular waveguide finline tapers, use was made, for the first time, of the powerful method of coupled modes [7] accompanied by the spectral-domain approach. It was shown that such a combination offers a very efficient computational scheme of the return and insertion losses of the "back-to-back" tapering transition. Unfortunately, experiments were unable to validate the presumed exact fields computations.

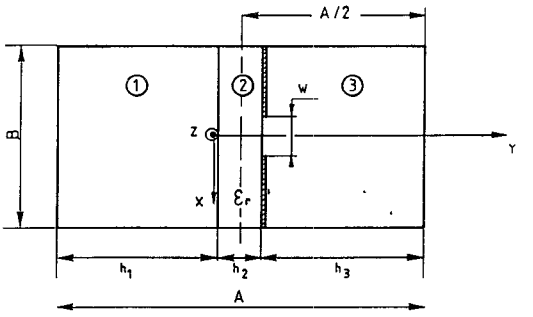

Fig. 1. Cross-section parameters of a unilateral finline. In the *Ku*-band (12–18 GHz), $A = 15.8$ mm, $B = 7.9$ mm, $h_2 = 0.635$ mm, and $\epsilon_r = 9.6$ (Alumina). In the *Ka*-band (26–40 GHz), $A = 7.112$ mm, $B = 3.556$ mm, $h_2 = 0.254$ mm, and $\epsilon_r = 2.22$ (Duroid 5880).

Recently, the transverse resonance techniques [8] were used to compute the resonant frequencies of a resonant structure containing the finline discontinuity and in consequence to determine the equivalent-circuit parameters of the discontinuity.

This paper presents a precise field theoretical solution of finline discontinuities using a combination of the spectral-domain approach and the modal analysis.

The aim of the paper is threefold: 1) to give an accurate evaluation of six eigenmodes of the unilateral finline via a thorough spectral-domain approach; 2) to perform calculations of the generalized scattering matrix of a single-step slot width discontinuity by combining the direct modal analysis and the spectral-domain approach [9] and, consequently, to determine the equivalent-circuit parameters of this discontinuity; 3) to compare the theory and experiments in the *Ku*- and *Ka*-bands on complex discontinuities [10], as this is the only method that enables the direct comparison of measured and calculated scattering parameters of either the simple or the complex discontinuity.

II. Spectral-Domain Approach of a Unilateral Finline

The axial field components $E_{z,i}(x, y)$ and $H_{z,i}(x, y)$ in the ith region ($i = 1, 2, 3$) are expanded in Fourier series (Fig. 1) within their domain

$$-B/2 \leqslant x \leqslant B/2.$$

Manuscript received February 12, 1985; revised May 31, 1985.

M. Helard is with the Centre Commun d'Etudes des Télécommunications et Télédivision, 35510 Cesson Sevigne, France.

J. Citerne is with the Laboratories Structures Rayonnantes, Department Genie Electrique, INSA, 35031 Rennes Cedex, France.

O. Picon and V. Fouad Hanna are with the Division Espace et Transmission Radioélectrique, Centre National d'Etudes des Télécommunications, 92131 Issy-Les-Moulineaux, France.

0018-9480/85/1000-0994$01.00 ©1985 IEEE

For odd waves, the following expansions of $E_{z,i}(x, y)$ and $H_{z,i}(x, y)$ are valid:

$$E_{zi}(x, y) = \sum_{m=1}^{\infty} \tilde{E}_{zi}(m, y) \sin \alpha_m x$$

$$H_{zi}(x, y) = \sum_{m=0}^{\infty} \tilde{H}_{zi}(m, y) \cos \alpha_m x \qquad (1)$$

where quantities with the sign ($\sim$) designate the line amplitude (i.e., the mth term of the Fourier series) associated with the space harmonic $\alpha_m = 2m\pi/B$.

The partial differential equations for the axial field components $E_{z,i}(x, y)$ and $H_{z,i}(x, y)$ are also Fourier expanded with respect to x; ordinary differential equations are derived for the mth line amplitudes $\tilde{E}_{z,i}(m, y)$ and $\tilde{H}_{z,i}(m, y)$, respectively.

For a unilateral finline (Fig. 1), these mth line amplitudes are given in Appendix I.

Through the application of boundary conditions at $y = 0$ and $y = h_2$, which are also Fourier expanded, the spectral coefficients are related to each other, to the mth line amplitudes of fin surface current components denoted $\tilde{J}_x(m, h_2)$ and $J_z(m, h_2)$, and to the mth line amplitude of the slot aperture field components denoted $\tilde{E}_x(m, h_2)$ and $\tilde{E}_z(m, h_2)$. Extensive algebraic manipulations of these boundary conditions then yield functional equations relating the mth line amplitude of the fin surface current components to the mth line amplitude of the slot aperture field components. For a unilateral finline, the standard computational scheme uses the following admittance matrix representations of these functional equations, namely:

$$\begin{bmatrix} G_{11} & G_{12} \\ G_{21} & G_{22} \end{bmatrix} \begin{bmatrix} \tilde{E}_x(m, h_2) \\ \tilde{E}_z(m, h_2) \end{bmatrix} = \begin{bmatrix} \tilde{J}_x(m, h_2) \\ \tilde{J}_z(m, h_2) \end{bmatrix}. \qquad (2)$$

Closed-form expressions of the $\bar{\bar{G}}$ matrix elements are listed in Appendix II.

Now it is the moment to start the numerical part through the application of the Galerkin's form of the general method of moments to the functional equations (2). The slot aperture field components $E_x(x, h_2)$ and $E_z(x, h_2)$ are expanded in terms of two complete sets of R and S basis functions denoted $\mathscr{E}_{x,r}(x, h_2)(r = 1, \cdots, R)$ and $\mathscr{E}_{z,s}(x, h_2)(s = 1, \cdots, S)$

$$E_x(x, h_2) = \sum_{r=1}^{R} a_r \mathscr{E}_{x,r}(x, h_2)$$

$$E_z(x, h_2) = \sum_{s=1}^{S} b_s \mathscr{E}_{z,s}(x, h_2). \qquad (3)$$

Obviously, the basis functions in (3) have nonzero values in the interval $-W/2 \leqslant x \leqslant W/2$ of the cell $-B/2 \leqslant x \leqslant B/2$.

The expansions (3) are displayed in Fourier series to bring the mth line amplitude of the aperture field components and the mth line amplitude of basis functions into relationship denoted by

$$\tilde{E}_x(m, h_2) = \sum_{r=1}^{R} a_r \tilde{\mathscr{E}}_{x,r}(m, h_2)$$

$$\tilde{E}_z(m, h_2) = \sum_{s=1}^{S} b_s \tilde{\mathscr{E}}_{z,s}(m, h_2). \qquad (4)$$

The coefficients a_r and b_s involved in (3) and (4) are the first true constants of the waveguide problem.

By using an inner product consistent with the Parseval theorem, the Galerkin's procedure is directly applied to the matrix form (2) in the Fourier domain. A set of $R + S$ homogeneous and linear equations, for which the $R + S$ unknowns are precisely the constants a_r and b_s, is obtained.

Nontrivial solutions of this set of equations occur for zero values of its matrix determinant. The real roots (i.e., $\beta^2 > 0$) determine the propagating eigenmodes, whereas the imaginary roots (i.e., $\beta^2 < 0$) determine evanescent ones.

For any given root β, the associated mth line amplitudes of the aperture field components are expressed in terms of the $R + S$ coefficients a_r and b_s involved in (4). By a substitution process of $\tilde{E}_x(m, h_2)$ and $\tilde{E}_z(m, h_2)$ in boundary conditions, the coefficients $A(m)$ through $H(m)$ are determined, as well as the mth line amplitude of the axial field components. The summation of Fourier series gives finally the axial field components of eigenmodes anywhere in the waveguide cross section.

Eigenmode normalization is not a necessary task as far as the waveguide treatment is concerned. However, this operation can be found relevant in the further discontinuity problem. So, applying again the Parseval's theorem, the orthogonality of eigenmodes in lossless waveguides can be expressed directly in the spectral domain as

$$\frac{B}{2} \sum_{m=0}^{\infty} \int_{-h_1}^{h_2+h_3} \left[\tilde{E}_{x,p}(m, y) \tilde{H}^*_{y,p'}(m, y) - \tilde{E}_{y,p}(m, y) \tilde{H}^*_{x,p'}(m, y) \right] dy = s \frac{\beta_p}{|\beta_p|} P \delta_{pp'} \qquad (5)$$

where δ_{pp} represents the Kroneker delta and the coefficient s can take the values $+1$ or -1 depending on the propagating or evanescent nature of the eigenmode labelled p. Line amplitudes of transverse field components involved in (5) are derived from longitudinal components given by (1). The eigenmode normalization is carried out if the $R + S$ unknowns a_r and b_r in (3) and (4) associated with a given root β are reevaluated to ensure a power flow value P equal to 1 W in (5).

III. Modal Analysis of Single- and Multiple-Step Slot Width Discontinuities

The problem to be treated is how an incident accessible power entering each side of the junction is apportioned between the various scattered eigenmodes. The solution lies in the derivation of the generalized scattering matrix [S] of the junction.

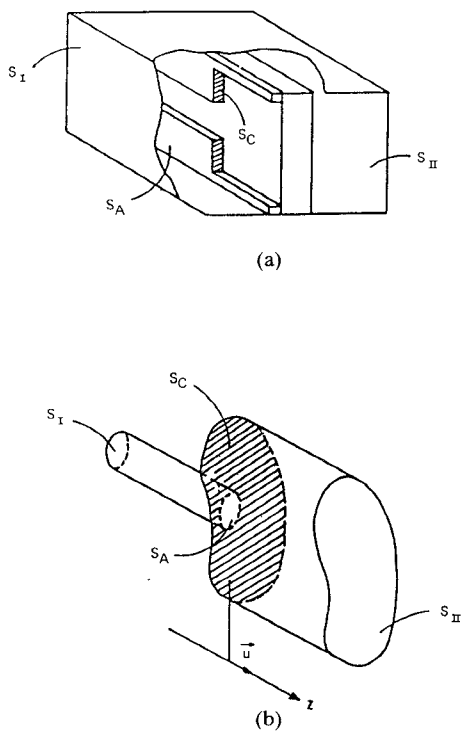

Fig. 2. (a) A single-step slot width junction between two unilateral finlines. (b) Model for modal analysis.

A single slot width discontinuity as that shown in Fig. 2(a) can be modeled by a junction between two cylindrical closed waveguides as shown in Fig. 2(b). We have to notice that the conducting fins in Fig. 2(a) have negligible thickness. They have been drawn so for a better comprehension of the model of Fig. 2(b).

The transverse electric and magnetic field to the left of the junction plane $z = 0$ (waveguide I side) can be expressed as

$$\vec{E}_T^{\,I} = \sum_{p=1}^{P} \left(A_p^I + B_p^I\right)\vec{e}_{p,T}^{\,I}$$

$$\vec{H}_T^{\,I} = \sum_{p=1}^{P} \left(A_p^I - B_p^I\right)\vec{h}_{p,T}^{\,I}. \tag{6}$$

In a similar manner, to the right of the junction plane $z = 0$, the expansion of the transverse electric and magnetic fields is written as

$$\vec{E}_T^{\,II} = \sum_{q=1}^{Q} \left(A_q^{II} + B_q^{II}\right)\vec{e}_{q,T}^{\,II}$$

$$\vec{H}_T^{\,II} = \sum_{q=1}^{Q} \left(B_q^{II} - A_q^{II}\right)\vec{h}_{q,T}^{\,II}. \tag{7}$$

The above expansions involve normalized transverse electric and magnetic fields $\vec{e}_{p,T}^{\,I}, \vec{h}_{p,T}^{\,I}$ (resp.: $\vec{e}_{q,T}^{\,II}, \vec{h}_{q,T}^{\,II}$) associated with the eigenmode p (resp.: q) of the waveguide I (resp.: II). Eigenmodes p and q are forward traveling waves in the two waveguides I and II, while the modal amplitudes A_p^I, B_p^I (resp. A_q^{II}, B_q^{II}) are referred to incident and reflected waves in the waveguide I (resp. II) at the junction plane.

If $S_I < S_{II}$ (this is the case outlined in Fig. 2), the boundary conditions at the junction plane $z = 0$ can be expressed as

$$\vec{E}_T^{\,I} = \vec{E}_T^{\,II} \tag{8a}$$

$$\vec{H}_T^{\,I} = \vec{H}_T^{\,II} \tag{8b}$$

on the aperture surface S_A and as

$$\vec{E}_T^{\,II} = 0 \tag{8c}$$

$$\vec{H}_T^{\,II} + \vec{J}_T^{\,I} \Lambda \vec{u} = 0 \tag{8d}$$

on the transverse conducting wall S_C.

The junction surfaces S_A and S_C are related to waveguide cross sections S_I and S_{II} by $S_A = S_I$ and $S_A + S_C = S_{II}$.

The surface current $\vec{J}_T^{\,I}$ on the conducting wall S_C is labeled with a subscript I to indicate a relationship with waveguide I.

The next step is to transform pairs of boundary functional equations (8a) and (8b) into an equivalent set of linear equations involving the $2(P + Q)$ modal amplitudes A_p^I, B_p^I, A_q^{II}, and B_q^{II} to be determined.

There is a unique procedure to derive such an equivalent linear set of $2(P + Q)$ equations that is closely related to the basic assumption $S_I < S_{II}$. This point has never been clarified enough in the literature, especially according to the uniqueness of the solution; therefore, it is summarized briefly in Appendix III.

Thus, the generalized scattering matrix of the simple discontinuity can be constructed from this system of equivalent linear equations which can be written in a matrix form as

$$^T[P]([A^I]+[B^I]) = [L]([A^{II}]+[B^{II}])$$
$$[K]([A^I]-[B^I]) = [N]([B^{II}]-[A^{II}]) \tag{9}$$

with

$$[A^I] = \begin{bmatrix} A_1^I \\ A_2^I \\ \vdots \\ A_p^I \\ \vdots \\ A_P^I \end{bmatrix} \quad [B^I] = \begin{bmatrix} B_1^I \\ B_2^I \\ \vdots \\ B_p^I \\ \vdots \\ B_P^I \end{bmatrix}$$

$$[A^{II}] = \begin{bmatrix} A_1^{II} \\ A_2^{II} \\ \vdots \\ A_q^{II} \\ \vdots \\ A_Q^{II} \end{bmatrix} \quad [B^{II}] = \begin{bmatrix} B_1^{II} \\ B_2^{II} \\ \vdots \\ B_q^{II} \\ \vdots \\ B_Q^{II} \end{bmatrix}. \tag{10}$$

where

$$[P] \text{ matrix } P \times Q;\ P_{p,q} = \int_{S_I} \vec{e}^{\,I}_{p,T} \Lambda \vec{h}^{\,II*}_{q,T} \cdot \vec{u}\, dS$$

$$[L] \text{ diagonal matrix } Q \times Q;\ L_{q,q} = S_q \frac{\beta_q}{|\beta_q|}$$

$$[K] \text{ diagonal matrix } P \times P;\ K_{p,p} = S_p \frac{\beta_p}{|\beta_p|}$$

$$[N] \text{ matrix } Q \times P;\ N_{q,p} = \int_{S_I} \vec{e}^{\,I*}_{p,T} \Lambda \vec{h}^{\,II}_{q,T} \cdot \vec{u}\, dS. \tag{11}$$

From (9), the generalized scattering matrix can be written in the form

$$[B] = [S] \cdot [A] \tag{12}$$

where

$$[B] = \begin{bmatrix} [B^I] \\ [B^{II}] \end{bmatrix} \quad [A] = \begin{bmatrix} [A^I] \\ [A^{II}] \end{bmatrix}. \tag{13}$$

The generalized scattering matrix of the junction assembles two reflection blocks denoted $[S_{11}]$ and $[S_{22}]$ and two transmission blocks denoted $[S_{21}]$ and $[S_{12}]$ arranged as

$$[S]_{S_I < S_{II}} = \begin{bmatrix} [S_{11}]_{S_I < S_{II}} & [S_{12}]_{S_I < S_{II}} \\ [S_{21}]_{S_I < S_{II}} & [S_{22}]_{S_I < S_{II}} \end{bmatrix}. \tag{14}$$

Each block has a size $(P+Q)\times(P+Q)$ and can be determined separately from matrices $[P]$, $[L]$, $[K]$, and $[N]$ after extensive algebraic manipulation of (9). Results are listed below:

$$\begin{aligned}
[S_{11}]_{S_I < S_{II}} &= \left([K] + [N]\cdot[L]^{-1}{}^T[P]\right)^{-1} \\
&\quad \cdot \left([K] - [N]\cdot[L]^{-1}{}^T[P]\right) \\
[S_{12}]_{S_I < S_{II}} &= 2\left([K] + [N]\cdot[L]^{-1}{}^T[P]\right)^{-1} \cdot [N] \\
[S_{21}]_{S_I < S_{II}} &= 2\left([L] + {}^T[P]\cdot[K]^{-1}\cdot[N]\right)^{-1}{}^T[P] \\
[S_{22}]_{S_I < S_{II}} &= -\left([L] + {}^T[P]\cdot[K]^{-1}\cdot[N]\right)^{-1} \\
&\quad \cdot \left([L] - {}^T[P]\cdot[K]^{-1}\cdot[N]\right).
\end{aligned} \tag{15}$$

The above $[S]$ matrix is labeled with subscripts $S_I < S_{II}$ to recall that it is addressed only to the case $S_I < S_{II}$. As mentioned in Appendix III, the $[S]$ matrix addressed to the alternative case $S_{II} < S_I$ is derived in a quite different way. However, the results can be related to the previously studied case: $S_I < S_{II}$. This relation can be written as

$$[S]_{S_I > S_{II}} = \begin{bmatrix} [S_{22}]_{S_I < S_{II}} & [S_{21}]_{S_I < S_{II}} \\ [S_{12}]_{S_I < S_{II}} & [S_{11}]_{S_I < S_{II}} \end{bmatrix}. \tag{16}$$

IV. Combination of the Spectral-Domain Approach and the Modal Analysis

The spectral-domain approach evaluates both the phase constants and the associated line amplitudes of eigenmode field components.

TABLE I
Basis Functions and Associated Line Amplitudes of the Aperture Field Corresponding to Odd Modes

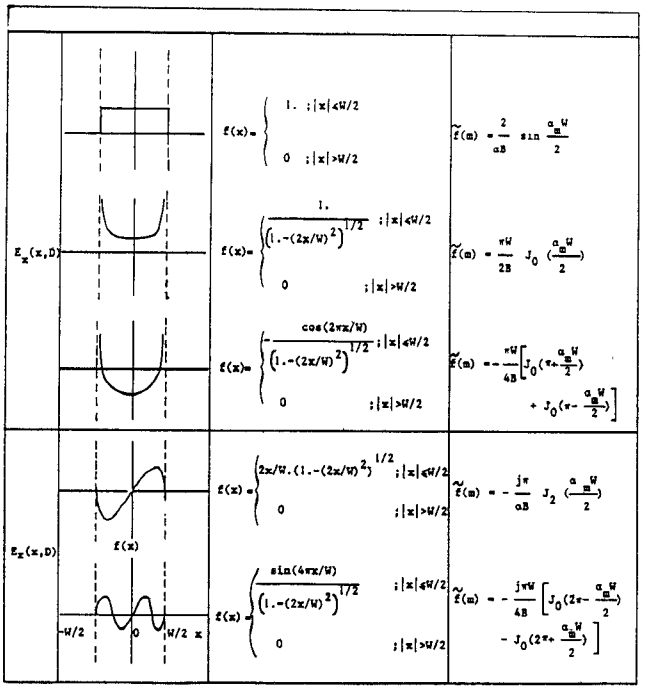

As a result of the eigenmode normalization, the calculation of elements L_{qq} and K_{pp} of matrices $[L]$ and $[K]$ is reduced to the determination of the propagating or evanescent nature of eigenmodes labeled p and q in waveguides I and II, respectively.

The computation of elements $P_{p,q}$ and $N_{q,p}$ of matrices $[P]$ and $[Q]$ can be quickly accomplished as it is done directly in the spectral domain. For example, the $P_{p,q}$ coefficient can be expressed from (11) as

$$P_{p,q} = B \sum_{m=0}^{\infty} \int_{-h_1}^{h_2+h_3} \left[\tilde{e}^{\,I}_{p,x}(m,y)\tilde{h}^{\,II*}_{q,y}(m,y) - \tilde{e}^{\,I}_{p,y}(m,y)\tilde{h}^{\,II*}_{q,x}(m,y)\right] dy. \tag{17}$$

V. Computed Results

A. Unilateral Finline Analysis

The sets of basis functions selected to describe the aperture field are represented in Table I. As shown in [11], the dominant mode can be described precisely by means of a single $E_x(x, D)$ basis function: the unit rectangular pulse denoted $f_1(x)$ in Table I. However, to describe both the dominant and the higher order modes, the aperture field expanded with the basis functions denoted $f_1(x)$, $f_2(x)$, $f_3(x)$, and $f_4(x)$ in Table I appears as a more judicious choice. Checks of this aperture field have been made in two limit cases for the unilateral finline: the standard rectangular waveguide ($\epsilon_r \to 1$; $W/B \to 1$) and the rectangular waveguide loaded symmetrically by a dielectric slab ($W/B \to 1$). They allowed conclusions to be made about the completeness of at least the first six eigenmodes.

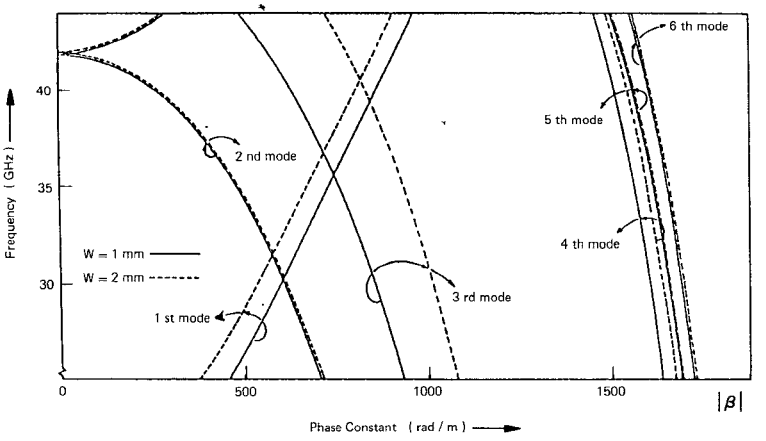

Fig. 3. Dispersion characteristics of eigenmodes in a unilateral finline in the *Ku*-band ($\epsilon_r = 2.22$, $h_2 = 0.254$ mm).

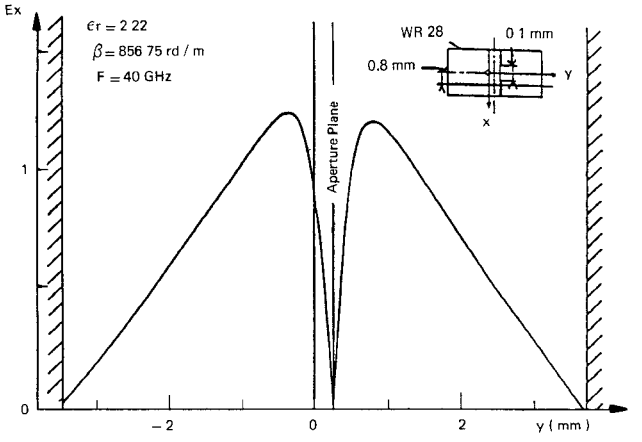

Fig. 4. E_x field component of the fundamental eigenmode for the shown finline.

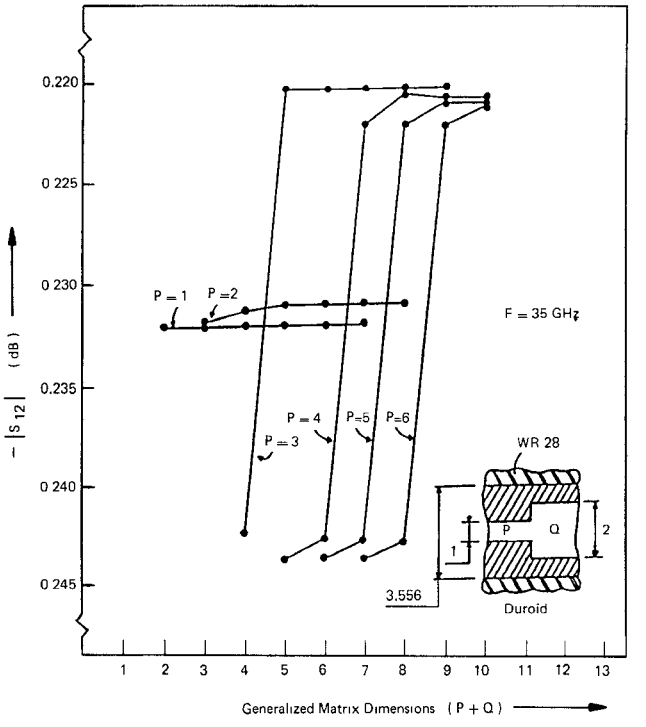

Fig. 5. Convergence test of the amplitude of the transmission coefficient for a step slot width discontinuity between two unilateral finlines (dimensions are in millimeters).

Dispersion characteristics of the first six eigenmodes in a unilateral finline in the *Ka*-band are plotted in Fig. 3 for two values of the slot width. They show that the frequency band for single-mode operation in a unilateral finline is quite identical to those of the standard WR28 rectangular waveguide. Another check of the aperture field is to compute the eigenmode distribution to be sure of the boundary conditions as shown in Fig. 4 for the E_x component of the fundamental mode as a function of y at $x = 0.8$ mm.

B. Scattering Parameters of Single-Step Slot Discontinuity in a Unilateral Finline

The most critical factor in the modal analysis is the convergence of reflection and transmission coefficients as a function of the number of modes taken into consideration when writing the boundary condition equations (8) at the junction plane. A relative convergence towards wrong values may be obtained if the number of modes is not sufficiently high.

Convergence tests on the moduli and the phases of reflection and transmission coefficients are performed making use of the description possibilities that are offered by the spectral-domain approach for the finline. The results of these tests applied on an abrupt junction between two finlines, as well as on an abrupt junction between a finline and a rectangular waveguide, are respectively given in Figs. 5 and 6. Here, the total number of modes did not exceed 14. The highest level of the curves drawn in Figs. 5 and 6 is supposed to be the real convergence level. Fig. 7 shows the computed scattering parameters of a unilateral finline discontinuity as a function of frequency compared with these computed by Schmidt [8] using the mode-matching procedure and with these computed by Sorrentino and Itoh [8] using the transverse resonance technique. Our results are in excellent agreement with Schmidt's results and in good agreement with Sorrentino's.

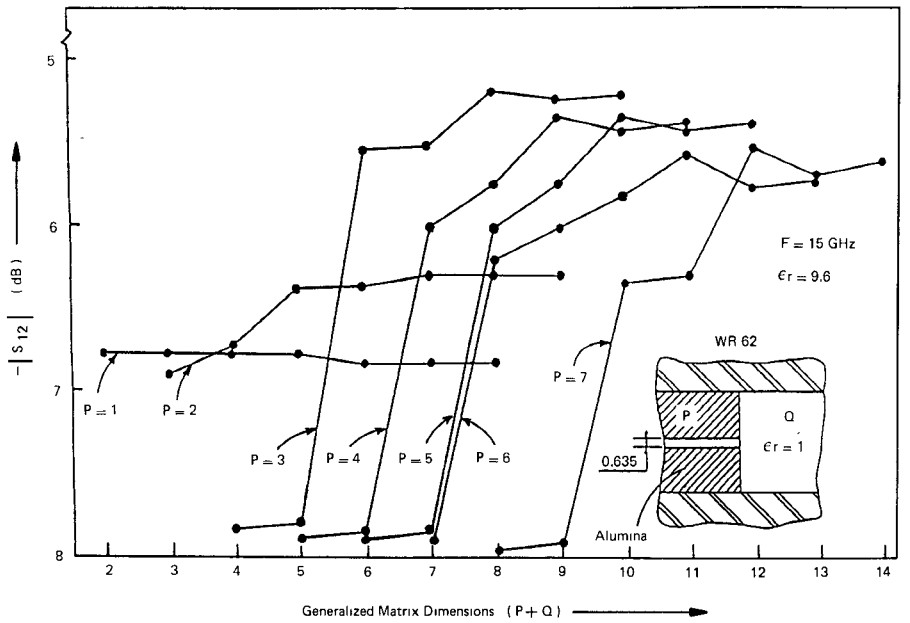

Fig. 6. Convergence test of the amplitude of the transmission coefficient for an abrupt junction between an empty rectangular waveguide and a unilateral finline (dimensions are in millimeters).

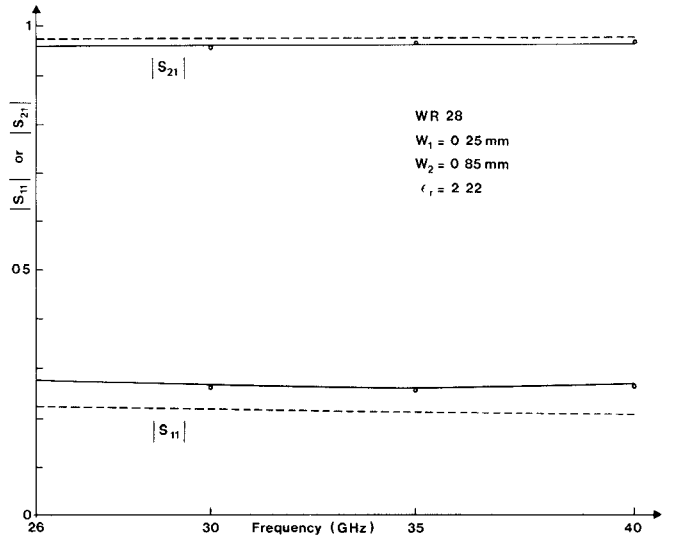

Fig. 7. Scattering parameters of a unilateral finline step discontinuity. —— Our theory, ----- Sorrentino's [8] results, and ∘ Schmidt's results.

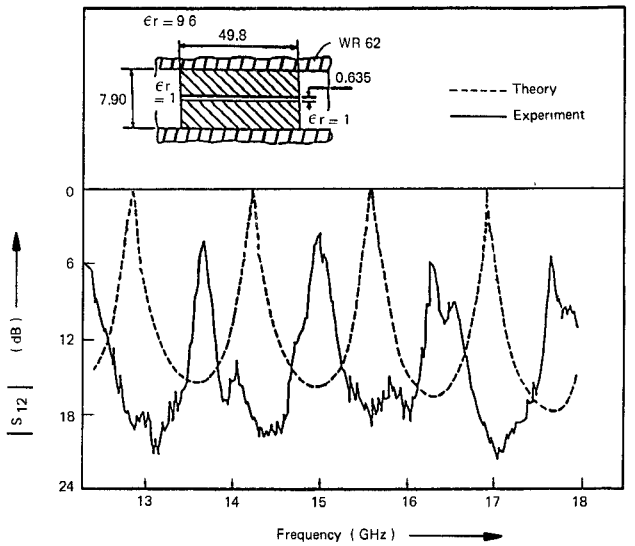

Fig. 8. Back-to-back arrangement of two abrupt junctions between an empty rectangular waveguide and a unilateral finline (dimensions are in millimeters.

C. Comparison Between Theory and Experiments

In order to evaluate objectively the effectiveness of the direct modal analysis for computer-aided design of finline circuits containing different discontinuities, the following three circuits have been fabricated, their scattering parameters have been calculated, and finally measured. The calculation of each circuit includes the effect of the discontinuity created by the narrow face of the substrate. The first circuit is that of two simple rectangular waveguide-unilateral finline junctions as shown in Fig. 8. The agreement can be judged satisfactory for the module of the transmission coefficient. The frequency shift of about 500 MHz can be explained by the mechanical constraints in the fabrication process (e.g., positioning grooves). The second circuit represents a pair of complex transitions each composed of three single simple transitions as shown in Fig. 9. The agreement between theory and experiment is still good in spite of the systematic frequency shift like that observed in the results of the first circuit. The third circuit is that given in Fig. 10, which represents a gradual transition operating in the *Ku*-band. The calculations are performed after dividing the transition into nine single simple discontinuities (Fig. 11). The agreement between theory and experiment is considered definitively satisfactory.

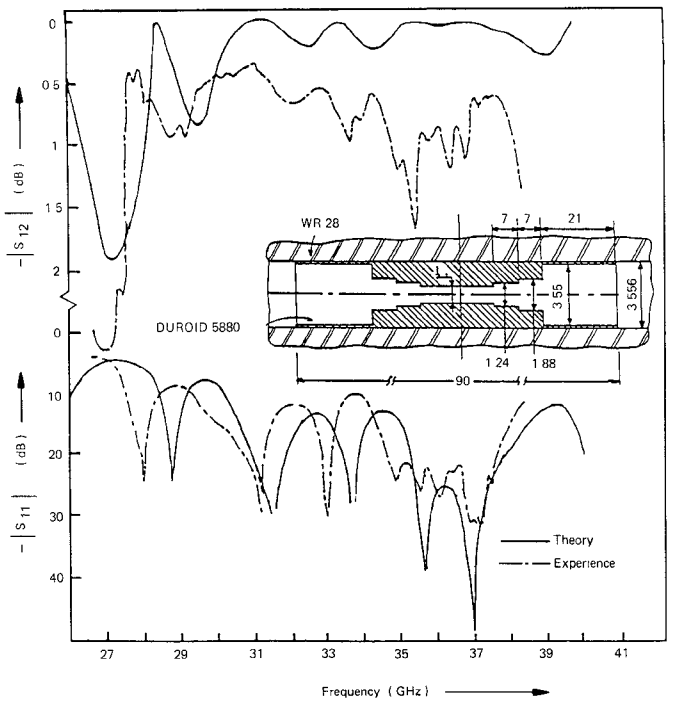

Fig. 9. Measurements and simulation results of a waveguide to finline complex transition in the *Ka*-band (dimensions are in millimeters).

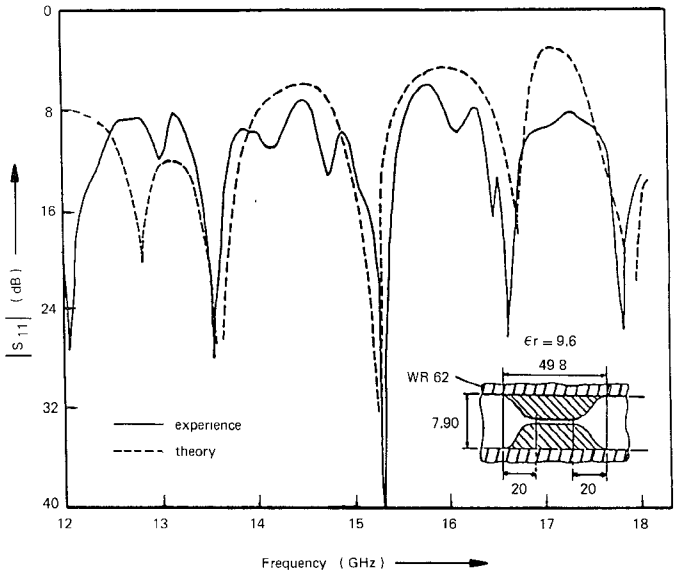

Fig. 10. Comparison between theory and experiment for the shown tapered transition (dimensions are in millimeters).

VI. Equivalent-Circuit Parameters of Simple Finline Discontinuities

The knowledge of both the reflection coefficient S_{11} and the transmission coefficient S_{21} in a given frequency band allows one to construct the equivalent circuit of the junction.

Each line having an access to the junction is considered as a lossless transmission line for which the effective dielectric constant and the characteristic impedance are those corresponding to the fundamental mode. The spectral-domain approach of a finline allows one to calculate these parameters directly in the spectral domain with excellent

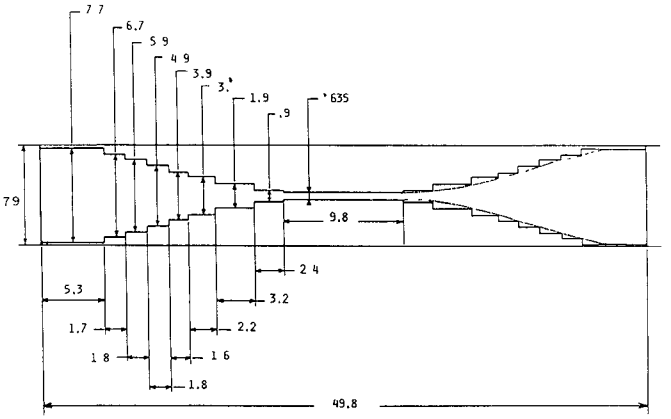

Fig. 11. Theoretical cutting used in the simulation of the transition reported in Fig. 10 (dimensions are in millimeters).

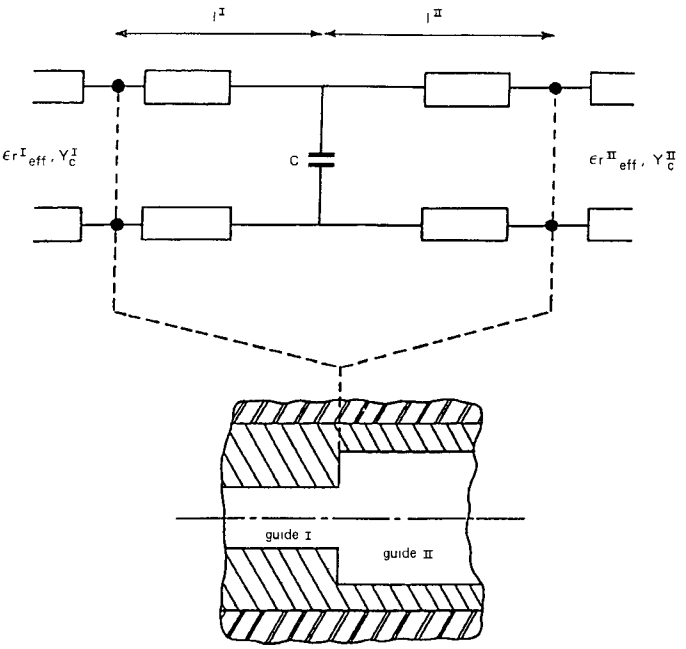

Fig. 12. Equivalent-circuit parameters of an elementary discontinuity.

accuracy. It is worth mentioning that the characteristic impedance is calculated according to a definition that relates the power flow of the fundamental mode and the potential that is induced between the slot edges.

As far as the single-step slot discontinuity is concerned, an equivalent circuit like that shown in Fig. 12 can be selected. The parameters C, l^{I}, and l^{II} of this equivalent circuit can be calculated by comparison of its scattering matrix to that of the single simple discontinuity restricted to four coefficients which represent the reflection and the transmission on only the fundamental eigenmodes of the two finlines having an access on the junction.

Examples of the results are reported in Figs. 13 and 14.

VII. Conclusion

The spectral-domain approach combined with the direct modal analysis appears as a very promising technique for calculation of scattering matrix elements of finline discontinuities.

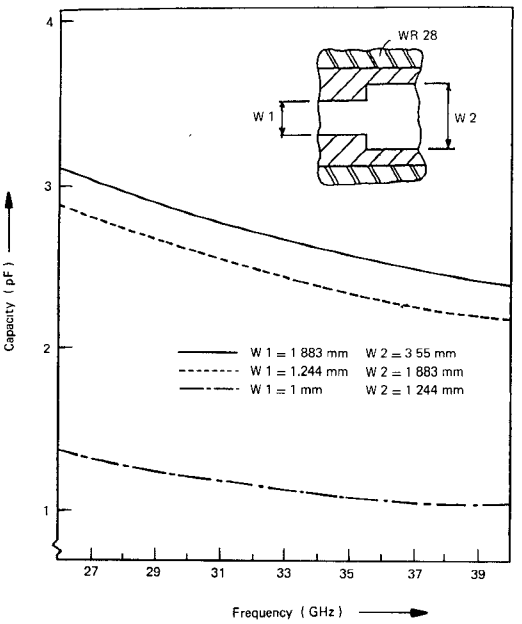

Fig. 13. Values of the lumped capacitance of the equivalent circuit of an elementary discontinuity as a function of frequency ($\epsilon_r = 2.22$, $h_2 = 0.254$ mm).

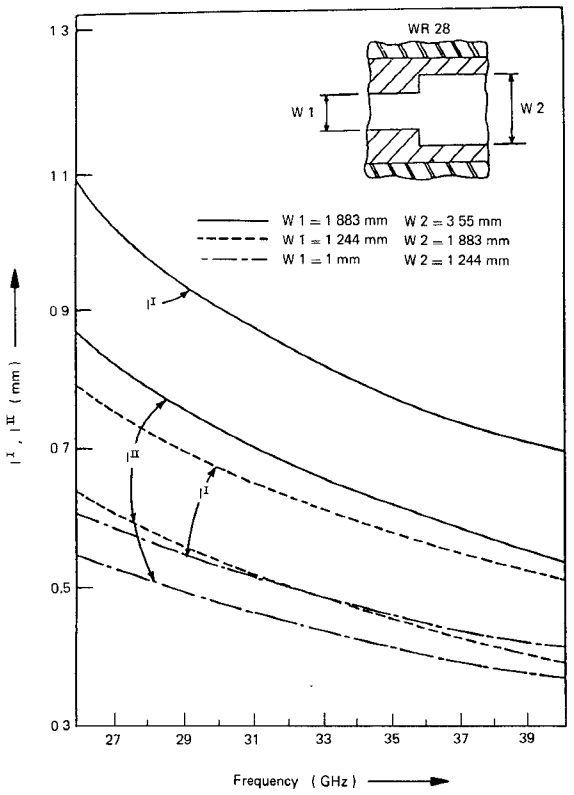

Fig. 14. Reference plane localization as a function of the frequency for the given elementary discontinuity ($\epsilon_r = 2.22$, $h_2 = 0.254$ mm).

Convergence is indeed necessary both in the waveguide eigenmode evaluation and in the waveguide discontinuity problem. In the case of a unilateral configuration, results show that a relatively simple aperture field allowed an unambiguous identification of six eigenmodes. Moreover, they show that, within such an identification, a satisfactory convergence on scattering parameters of a step slot width discontinuity can be achieved.

The agreement between theory and measurements performed on three different complex finline discontinuities is quite satisfactory.

Appendix I

The mth line amplitudes $\tilde{E}_{z,i}(m, y)$ and $\tilde{H}_{z,i}(m, y)$ can be written in the case of unilateral finline in the following form:

$$\tilde{E}_{z,1}(m, y) = A(m)\sinh\gamma_1(y + h_1)$$
$$\tilde{H}_{z,1}(m, y) = B(m)\cosh\gamma_1(y + h_1) \qquad \text{(A1a)}$$

in region (2)

$$\tilde{E}_{z,2}(m, y) = C(m)\sinh\gamma_2 y + D(m)\cosh\gamma_2 y$$
$$\tilde{H}_{z,2}(m, y) = E(m)\sinh\gamma_2 y + F(m)\cosh\gamma_2 y \qquad \text{(A1b)}$$

and in region (3)

$$\tilde{E}_{z,3}(m, y) = G(m)\sinh\gamma_3(h_2 + h_3 - y)$$
$$\tilde{H}_{z,3}(m, y) = H(m)\cosh\gamma_3(h_2 + h_3 - y) \qquad \text{(A1c)}$$

where coefficients γ_i ($i = 1$, 2, and 3) are defined as

$$\gamma_1^2 = \gamma_3^2 = \alpha_m^2 - k_1^2$$
$$\gamma_2^2 = \alpha_m^2 - k_2^2 \qquad \text{(A2a)}$$

with

$$k_1^2 = \omega^2\mu_0\epsilon_0 - \beta^2$$
$$k_2^2 = \omega^2\mu_0\epsilon_0\epsilon_r - \beta^2 \qquad \text{(A2b)}$$

represent the transverse wavenumbers of the mth line amplitude of the guided wave inside each region.

In (A2b), β denotes the phase constant of the guided wave to be determined at any given angular frequency ω.

Appendix II

The elements of the admittance matrix representation $[G]$ given in (2) can be written as

$$G_{11} = -j\left[k_2^2\frac{\tanh(\gamma_2 h_2)}{\mu_0\omega\gamma_2} - \epsilon_0 F\left(k_2^2\frac{\gamma_1}{\tanh(\gamma_1 h_1)} + k_1^2\frac{\epsilon_r\gamma_2}{\tanh(\gamma_2 h_2)}\right) + k_1^2\frac{\coth(\gamma_1 h_3)}{\mu_0\omega\gamma_1}\right] \qquad \text{(A3)}$$

$$G_{12} = G_{21} = j\alpha\beta\left[\frac{\tanh(\gamma_2 h_2)}{\mu_0\omega\gamma_2} - \epsilon_0 F\left(\frac{\gamma_1}{\tanh(\gamma_1 h_1)} + \frac{\epsilon_r\gamma_2}{\tanh(\gamma_2 h_2)}\right) + \frac{\coth(\gamma_1 h_3)}{\mu_0\omega\gamma_1}\right] \qquad \text{(A4)}$$

$$G_{22} = j\left[B_2\left(\frac{\tanh(\gamma_2 h_2)}{\mu_0\omega\gamma_2} - F\frac{\epsilon_0\gamma_1}{\tanh(\gamma_1 h_1)}\right) + B_1\left(\frac{\coth(\gamma_1 h_3)}{\mu_0\omega\gamma_1} - F\frac{\epsilon_0\epsilon_r\gamma_2}{\tanh(\gamma_2 h_2)}\right)\right] \qquad \text{(A5)}$$

where

$$k_2^2 = \omega^2\mu_0\epsilon_0\epsilon_r - \beta^2$$

$$k_1^2 = \omega^2\mu_0\epsilon_0 - \beta^2$$

$$B_2 = \alpha^2 - \mu_0\epsilon_0\epsilon_r\omega^2$$

$$B_1 = \alpha^2 - \mu_0\epsilon_0\omega^2$$

$$F = \frac{k_1^2 k_2^2}{\cosh^2(\gamma_2 h_2)} \cdot \frac{\omega}{\delta}$$

$$\delta = (\alpha\beta)^2\left(k_1^2 - k_2^2\right)^2 - \epsilon_0\mu_0\omega^2\left[k_1^4\epsilon_r\gamma_2^2 + k_2^4\gamma_1^2 + (k_1k_2)^2\gamma_1\gamma_2\left(\frac{\tanh(\gamma_2 h_2)}{\tanh(\gamma_1 h_1)} + \epsilon_r\frac{\tanh(\gamma_1 h_1)}{\tanh(\gamma_2 h_2)}\right)\right].$$

Appendix III

Equations (8a) and (8c) are scalarly multiplied by $\vec{h}^{\mathrm{II}*}_{q,T}\Lambda\vec{u}$ and $e^{\mathrm{I}*}_{p,T}\Lambda\vec{u}$, respectively, and then integrated over S_A. Since $S_{\mathrm{I}} < S_{\mathrm{II}}$, $S_A = S_{\mathrm{I}}$, thus the orthogonality properties of eigenmodes in waveguide I can be used to obtain the following set of $P+Q$ linear equations:

$$\sum_{p=1}^{P}\left(A_p^{\mathrm{I}} + B_p^{\mathrm{I}}\right)\int_{S_{\mathrm{I}}}\vec{e}^{\mathrm{I}}_{p,T}\Lambda\vec{h}^{\mathrm{II}*}_{q',T}\vec{u}\,dS =$$

$$\sum_{q=1}^{Q}\left(A_q^{\mathrm{II}} + B_q^{\mathrm{II}}\right)\int_{S_{\mathrm{I}}}\vec{e}^{\mathrm{II}}_{q,T}\Lambda\vec{h}^{\mathrm{II}*}_{q',T}\vec{u}\,dS, \qquad q'=1,\cdots,Q \quad \text{(A6)}$$

$$S_{p'}\frac{\beta^{\mathrm{I}}_{p'}}{|\beta_{p'}|}\left(A^{\mathrm{I}}_{p'} - B^{\mathrm{I}}_{p'}\right) = \sum_{q=1}^{Q}\left(B_q^{\mathrm{II}} - A_q^{\mathrm{II}}\right)\int_{S_{\mathrm{I}}}\vec{e}^{\mathrm{I}*}_{p',T}\Lambda\vec{h}^{\mathrm{II}}_{q,T}\vec{u}\,dS,$$

$$p'=1,\cdots,P \quad \text{(A7)}$$

which are found quite equivalent to boundary functional equations (8).

Similarly, the scalar multiplication of (8b) by $h^{\mathrm{II}*}_{q,T}\Lambda\vec{u}$ and (8d) by $e^{\mathrm{I}*}_{p,T}\Lambda\vec{u}$ and the surface integration over S_C provides the set of $P+Q$ equations

$$\sum_{q=1}^{Q}\left(A_q^{\mathrm{II}} + B_q^{\mathrm{II}}\right)\int_{S_C}\vec{e}^{\mathrm{II}}_{q,T}\Lambda h^{\mathrm{II}*}_{q,T}\cdot\vec{u}\,dS = 0,$$

$$q'=1,\cdots,Q \quad \text{(A8)}$$

$$\sum_{q=1}^{Q}\left(B_q^{\mathrm{II}} - A_q^{\mathrm{II}}\right)\int_{S_C}\vec{e}^{\mathrm{I}*}_{p',T}\Lambda\vec{h}^{\mathrm{II}}_{q,T}\cdot\vec{u}\,dS = 0,$$

$$p'=1,\cdots,P. \quad \text{(A9)}$$

During derivation, use has been made of the following equation:

$$\int_{S_C}\left(\vec{e}_{p',T}\Lambda\vec{u}\right)\cdot\left(\vec{J}^{\mathrm{I}}_T\Lambda\vec{u}\right)dS = \int_{S_C}\vec{J}^{\mathrm{I}}_T\cdot e^{\mathrm{I}*}_{p'T}\,dS = 0$$

due to the above-mentioned connection of the surface current $\vec{J}^{\mathrm{I}}_T$ with waveguide I.

Clearly, the set (A8) can be imbedded in set (A6) after enlarging the surface integration at its right-hand side from S_{I} to $S_{\mathrm{II}} = S_A + S_C$. Such a widening is done without altering the left-hand side of set (A6), and, moreover, use can then be made of the orthogonality in waveguide II.

Now, as far as the set (A7) is concerned, another look at the set (A9) shows that its right-hand side already includes it.

Considering now the case $S^{\mathrm{I}} > S^{\mathrm{II}}$, the functional boundary conditions of (8) still hold except those over S_C ((8c) and (8d)), which must be replaced by

$$E^{\mathrm{I}}_T = 0 \quad \text{(A10)}$$

$$\vec{H}^{\mathrm{I}}_T = \vec{J}^{\mathrm{II}}_T\Lambda\vec{u} \quad \text{(A11)}$$

where the superscript II of the surface current notation $\vec{J}^{\mathrm{II}}_T$ indicates now a relationship with the waveguide II. There, another unique procedure must be employed to derive the linear set of $P+Q$ equations equivalent to the boundary functional equations (8), (A9), and (A10).

This alternative procedure starts from the scalar multiplication of (8a) and (A6) by $h^{\mathrm{I}*}_{p',T}\Lambda\vec{u}$ and of (8b) and (A7) by $e^{\mathrm{II}*}_{q'T}\Lambda\vec{u}$, followed by surface integration where use must be made of the basic assumptions $S_A = S_{\mathrm{II}}$ and $S_A + S_C = S_{\mathrm{I}}$.

References

[1] K. Solbach, "The status of printed millimeter-wave *E*-plane circuits," *IEEE Trans. Microwave Theory Tech.*, vol. MTT-31, pp. 107–121, Feb. 1983.

[2] A. Wexler, "Solution of waveguide discontinuities by modal analysis," *IEEE Trans. Microwave Theory Tech.*, vol. MTT-15, pp. 508–517, Sept. 1967.

[3] H. El Hennaway and K. Schunemann, "Analysis of finline discontinuities," in *Proc. 9th Eur. Microwave Conf.* (Brighton, England), 1979, pp. 448–452.

[4] H. Hofmann, "Dispersion of planar waveguides for millimeter-wave application," *Arch. Elek. Übertragung.*, vol. 31, pp. 40–44, Jan. 1977.

[5] H. El Hennaway and K. Schunemann, "Computer-aided design of finline detectors, modulators and switches," *Arch. Elek. Übertragung.*, vol. 36, pp. 49–56, Feb. 1982.

[6] A. Beyer and I. Wolff, "Calculation of transmission properties of inhomogeneous finlines," in *Proc. 10th Eur. Microwave Conf.* (Warsaw, Poland), 1980, pp. 322–326.

[7] D. Mirshekar-Syahkal and J. B. Davies, "Accurate analysis of tapered planar transmission lines for microwave integrated circuits," *IEEE Trans. Microwave Theory Tech.*, vol. MTT-29, pp. 123–128, Feb. 1981.

[8] R. Sorrentino and I. Itoh, "Transverse resonance analysis of finline discontinuities," *IEEE Trans. Microwave Theory Tech.*, vol. MTT-32, pp. 1633–1638, Dec. 1984.

[9] M. Helard, J. Citern, O. Picon, and V. Fouad Hanna, "Exact calculation of scattering parameters of a step slot width discontinuity in a unilateral finline," *Electron. Lett.*, vol. 14, pp. 537–539, July 1983.

[10] M. Helard, J. Citern, O. Picon, and V. Fouad Hanna, "Solution of finline discontinuities through the identification of its first four higher order modes," in *IEEE MTT-S Int. Microwave Symp. Dig.*, May 1983, pp. 387–389.

[11] J. B. Knorr and P. M. Shayda, "Millimeter wave finline characteristics," *IEEE Trans. Microwave Theory Tech.*, vol. MTT-28, pp. 737–742, July 1980.

✠

Maryline Helard was born in Argentan, France, on April 18, 1958. She received the degree of electrical engineering from the National Institute of Applied Sciences (INSA), at Rennes, in 1981. From 1982 to 1985, she was a Research Assistant at the Microwave Laboratory (UA CNRS N° 834) at this Institute. In 1984, she received the doctorate degree in electrical engineering after writing her dissertation on finline discontinuity analysis.

She joined, in March 1985, the Common Centre of Studies in Telecommunication and Telediffusion at Rennes (CCETT).

✠

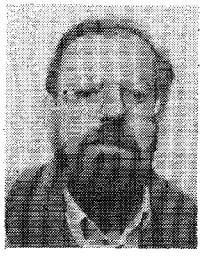

Jacques Citerne was born in Arras, France, on October 5, 1945. He received the doctor in physics degree in 1978 from the Technical University of Lille, France.

From 1978 to 1980, he held the leadership of the Propagation and Circuit Group of the Microwave and Semiconductor Center at the same university. Since 1980, he has been Professor of Electrical Engineering at the National Institute of Applied Sciences (INSA) at Rennes, France, where he created a Microwave Laboratory, which is now supported by the French National Center of Scientific Research (UA CNRS 834). The laboratory is currently working on various problems related to microwave integrated circuitry in centimeter- and millimeter-waves, with a special stress on the role of discontinuities in the design of open and closed passive components.

Odile Picon was born in Paris, France, on March 31, 1951. She received the "Agregation of Physic," prepared in the "Ecole Normale Supérieure de Fontenay-aux-Roses," France, in 1976, and the doctor degree (Doctorat de 3ème cycle) in external geophysics, in 1980, from the University of Orsay, France.

Since 1982, she has been a Research Engineer in the Space and Radioelectric Transmission Division of the "Centre National d'Etudes des Telecommunications." Her research work deals with electromagnetic theory and, particularly, with finline discontinuity analysis.

✠

Victor Fouad Hanna received the B.Sc. degree (honors) in electronic engineering from Cairo University, Cairo, Egypt, in 1965, and the M.Sc. degree in microwave engineering from Alexandria University, Alexandria, Egypt, in 1969. He received the D.Sc. degree [Doctorat ès Sciences Physiques (doctorat d'Etat)] from "l'Institut National Polytechnique (I.N.P.)," Toulouse, France, in 1975.

He was a Research Assistant in the National Research Center, Cairo, Egypt, and the microwave laboratory of the "I.N.P.," Toulouse, France, from 1965–1970 and 1970–1975, respectively. From 1975 to 1979, he was a Researcher in the Electrical and Electronics Engineering Laboratory, National Research Center, Cairo, Egypt, engaged in research in the field of microwave theory and techniques and microwave solid-state devices. From 1979 till now, he has been a Research Engineer in the Space and Radioelectric Transmission Division of the "Centre National d'Etudes des Télécommunications," France. His current research interests deal with electromagnetic theory, numerical methods for solving field problems, characterization of microstrip-like transmission lines, and millimeter-wave transmission lines.